

Jamison Assunção Victor Sacek

Department of Geophysics, Universidade de São Paulo  
Instituto de Astronomia, Geofísica e Ciências Atmosféricas

INSTITUTO DE ASTRONOMIA,  
GEOFÍSICA E CIÊNCIAS  
ATMOSFÉRICAS

## Introduction

The Pantanal wetland (Figure 1) is a Quaternary basin in Southwestern Brazil, reaching up to  $\sim 500$  m of sedimentary package. Although the relatively recent formation of the basin, the mechanisms involved in the origin of the regional subsidence are not fully understood. Previous works proposed a flexural origin for the basin, invoking the last pulse of Andean tectonism and consequent topographic load as the source for the creation of the Pantanal Basin. However, taking into account the flexural rigidity of the South American lithosphere and the Andean geometry, it is difficult to explain the subsidence amplitude as well as the position of the basin due to flexural effects. Therefore, probably another mechanism must be involved in the formation and evolution of this active sedimentary basin.

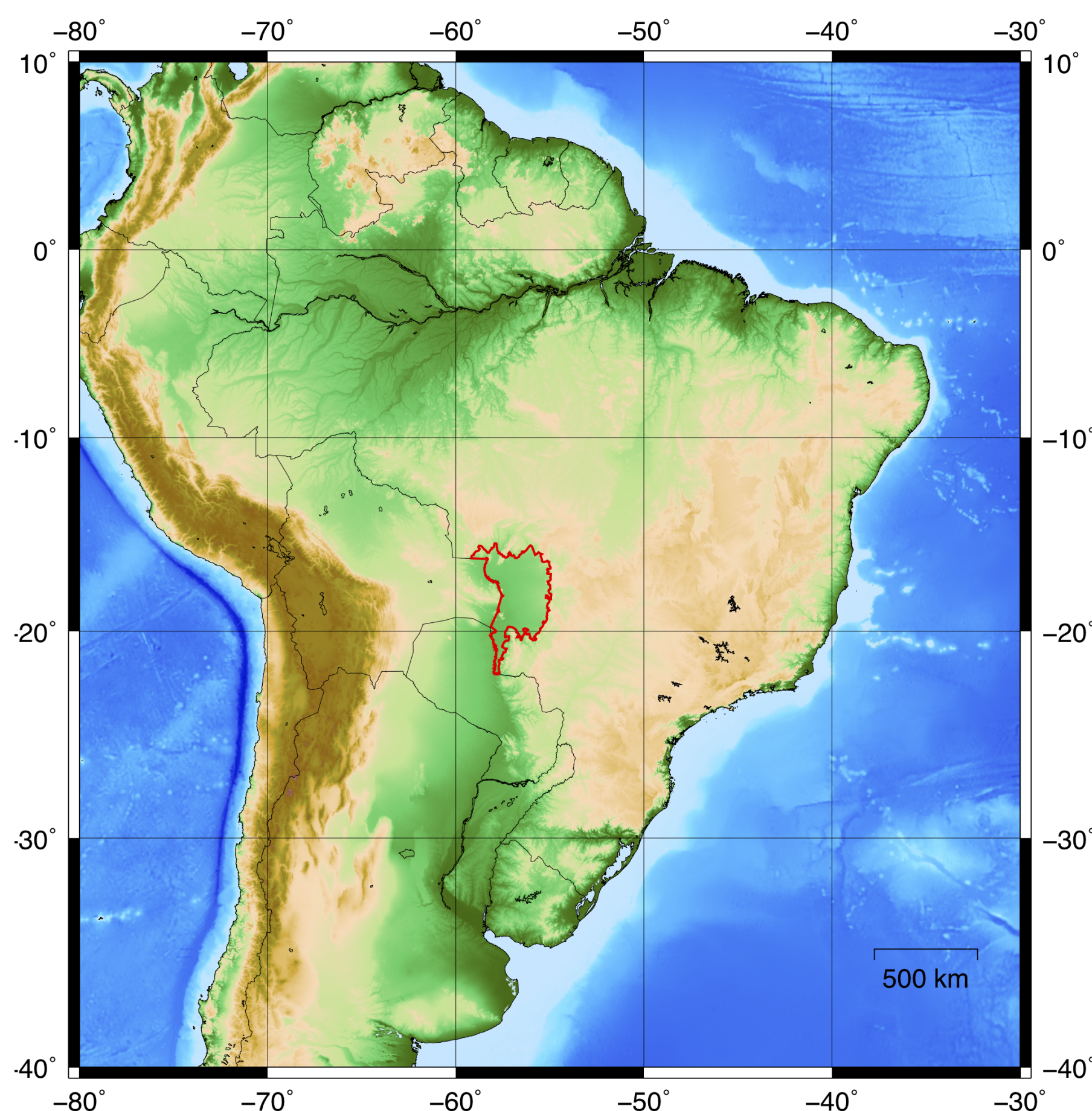


Figure 1: Map of South America showing the Pantanal Basin perimeter.

In the present work we will perform several 2D numerical simulations to evaluate how initial conditions can contribute to the buoyancy of the subducting Nazca plate. The results will be used in an upcoming study to calculate the influence of mantle convection generated by the subducting slab geometry and assess if it can induce dynamic topography and contribute to create the depression associated with the Pantanal Basin.

We used a finite element code to simulate the thermochemical convection in the mantle, calculating the associated dip angle of subduction along a profile from  $80.0^{\circ}\text{W}$  to  $48.5^{\circ}\text{W}$ , crossing the Pantanal wetland at a latitude of  $18^{\circ}\text{S}$ . To simulate the mantle flow, the thickness of both lithosphere and crust were resampled from the global LITHO1.0 model and the initial thermal structure for subducting slab was constructed based on a simplified thermokinematic model. The subducting slab geometry adopted was derived from the Slab2 model. The results will be considered to three dimensional models in the future to better represent latitudinal variations of the subducting slab and consequently improve the representation of the dynamic topography in the interior of the South American Plate.

## Numerical Methods

We used the 3D finite element numerical code MD3D [5] to solve the Stokes flow for a fluid using the Boussinesq approximation in a Cartesian coordinate system. This resulted in the equations for conservation of mass (Equation 1), momentum (Equation 2) and energy (Equation 3) [8].

$$u_{i,i} = 0 \quad (1)$$

$$\sigma_{ij,j} + g\alpha\rho_0 T\delta_{ij} = 0 \quad (2)$$

$$\frac{\partial T}{\partial t} + u_i T_{,i} = \kappa T_{,ii} \quad (3)$$

where  $u_i$  is the velocity in the  $i$  direction,  $\sigma_{ij,j}$  is the stress tensor (Equation 4),  $g$  is the acceleration of gravity,  $\rho_0$  is the mantle reference viscosity,  $\alpha$  is the coefficient of thermal expansivity,  $T$  is temperature,  $\delta_{ij}$  is the Kronecker delta function,  $t$  is time, and  $\kappa$  is the thermal diffusivity.

$$\sigma_{ij,j} = -P\delta_{ij} + \eta(u_{i,j} + u_{j,i}) \quad (4)$$

where  $P$  is the dynamic pressure, and  $\eta$  is the viscosity.

## Initial conditions

To study how the buoyancy changes as a function of the initial parameters, the length of the subducting oceanic lithosphere will be reduced to match the depth of 450 km and we will simulate for 5 Myr until it "recovers its original length. This will serve as well to allow flow beneath the subducting plate, restricted to the longitudinal direction.

### Layer model

The chosen layer model for the simulations is a combination of the Slab2 model [2] and the LITHO1.0 model [4] (Figure 2). While the Slab2 provides data for the geometry of the subducting slab, the LITHO1.0 provides information about the thickness of the crust and the depth of the lithosphere-asthenosphere boundary (LAB).

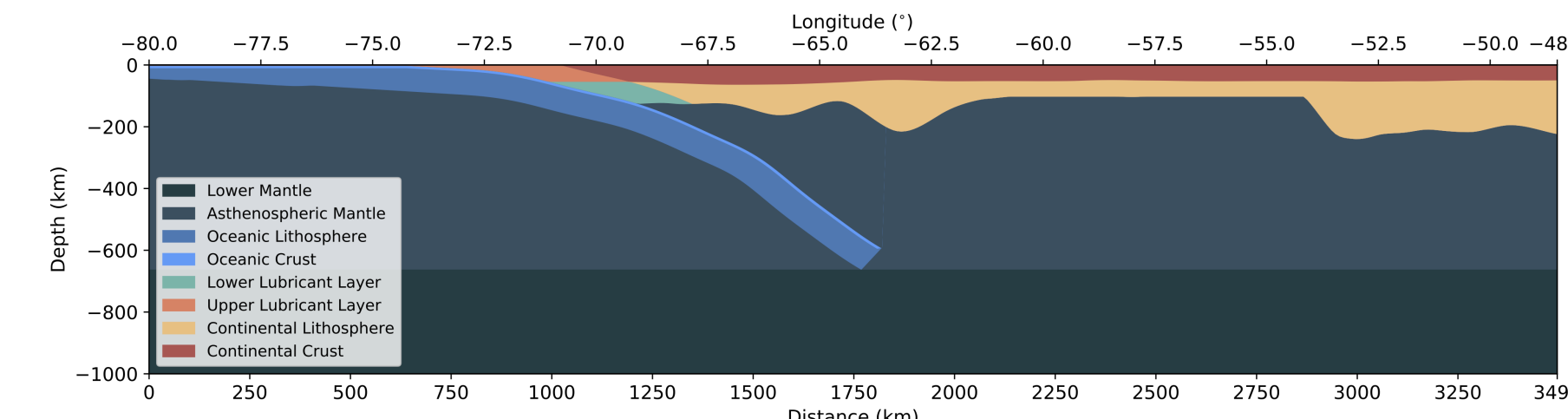


Figure 2: Example of an initial layer model with minimum LAB depth of 100 km in the continental regions and maximum oceanic crust depth of 8 km. Dipping subducting slab has a thickness of 85.5 km with an oceanic crust 8 km thick.

### Thermal structure

The lithosphere temperature is assumed to increase with depth for both continental and oceanic regions. It starts at  $0^{\circ}\text{C}$  at the surface and increases linearly until  $1300^{\circ}\text{C}$  at the bottom of the lithosphere. For the asthenosphere, the geothermal gradient respects the adiabatic relation shown in Equation 5.

$$T(z) = (T_0 - 273.15) \exp \frac{\alpha g z}{C_p} \quad (5)$$

where  $T_0$  is the potential temperature of the mantle on the surface,  $\alpha = 3.28 \cdot 10^{-5} \text{ K}^{-1}$  is the thermal expansion coefficient,  $g = 9.8 \text{ m/s}^2$  is the gravity acceleration, and  $C_p = 1250 \text{ m}^2/\text{K s}^2$  is the heat capacity.  $T_0$  is defined such that the temperature on the bottom of the model is  $1518.68^{\circ}\text{C}$ . This value is chosen to make the viscosity at that depth equals to  $10^{19} \text{ Pa s}$ .

For the subducting oceanic slab, we consider a semi-infinite slab of velocity  $v$  descending into an isothermal mantle and solved Equation 3 for  $\partial T/\partial t = 0$ . Furthermore, we added a contribution  $\delta T = T(z) - T_0$ , which is the difference between the potential temperature of the mantle on the surface and the temperature  $T(z)$  at a certain depth  $z$ .

To simulate the heat conduction during before the simulation, we diffused the thermal structure for 20 Myr using the boundary condition of  $\partial T/\partial x = 0$  on the sides of the model.

### Velocity field

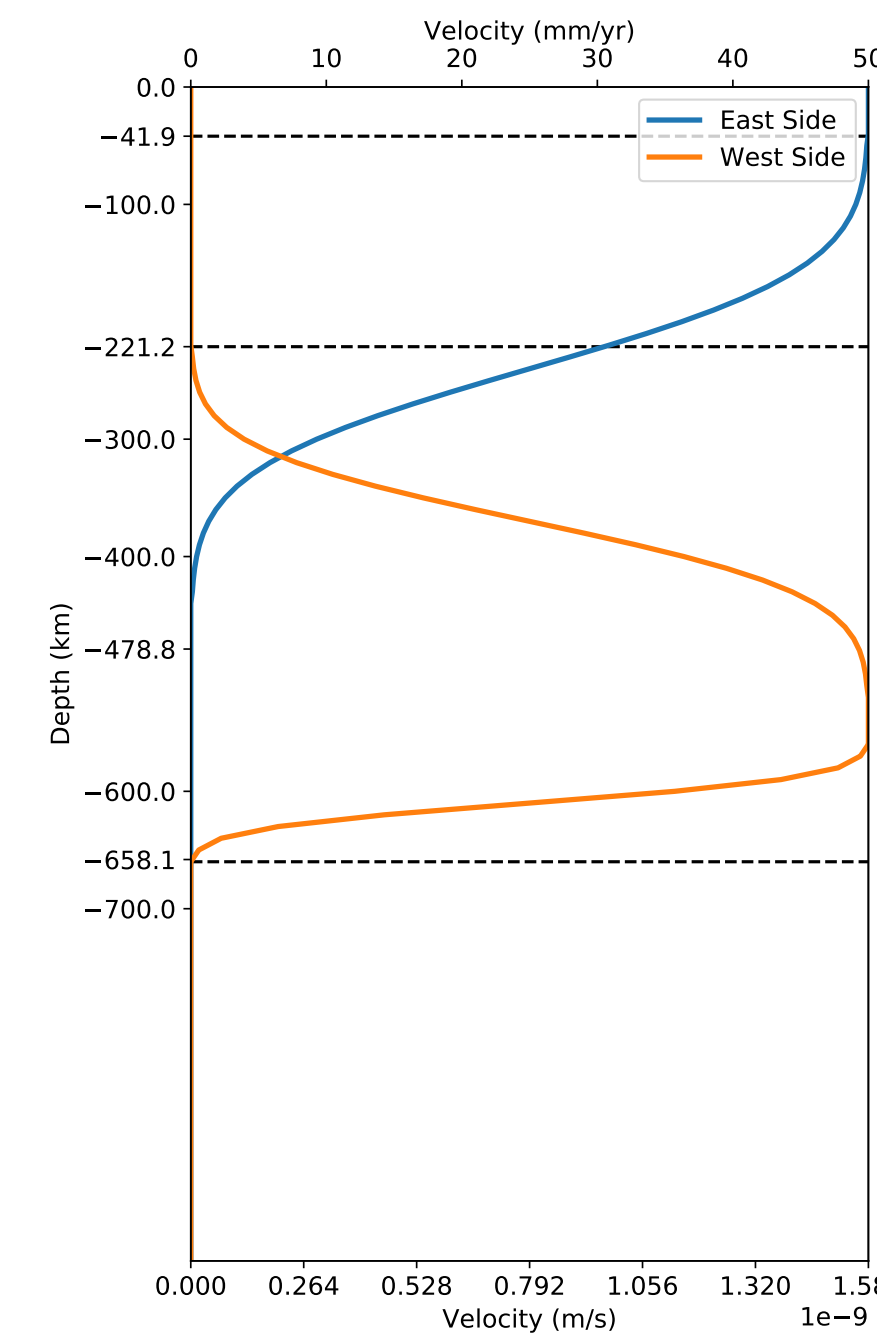


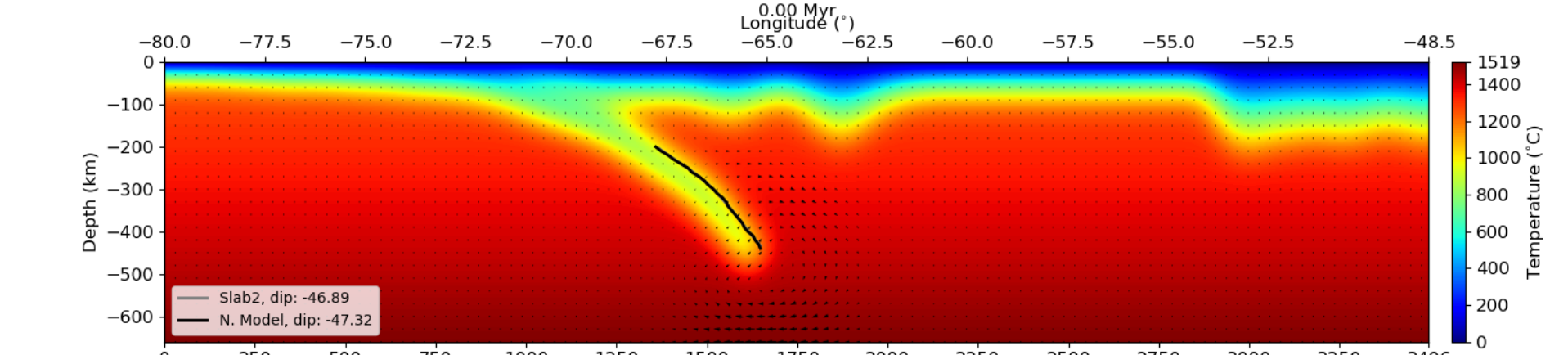
Figure 3: Example of an initial velocity field where the oceanic lithosphere is 41.9 km thick on the west side of the model and the continental lithosphere is 221.2 km thick on the east side of the model.

### Rheology model

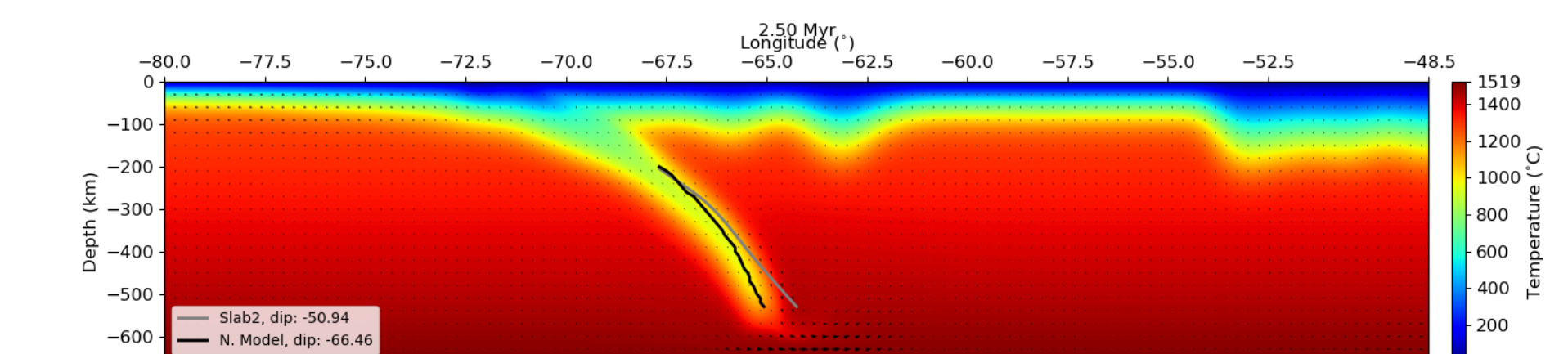
The viscosity will be considered to vary exponentially as a function of the temperature  $T$  and a compositional factor  $C$  as in the Frank-Kamenetskii approximation (Equation 6). We consider the mantle to be a fluid of variable viscosity for a steady state ductile creep, as it is usually considered for thermochemical convection [6].

$$\eta(T, C) = C\eta_r b^* \exp(-\gamma T) \quad (6)$$

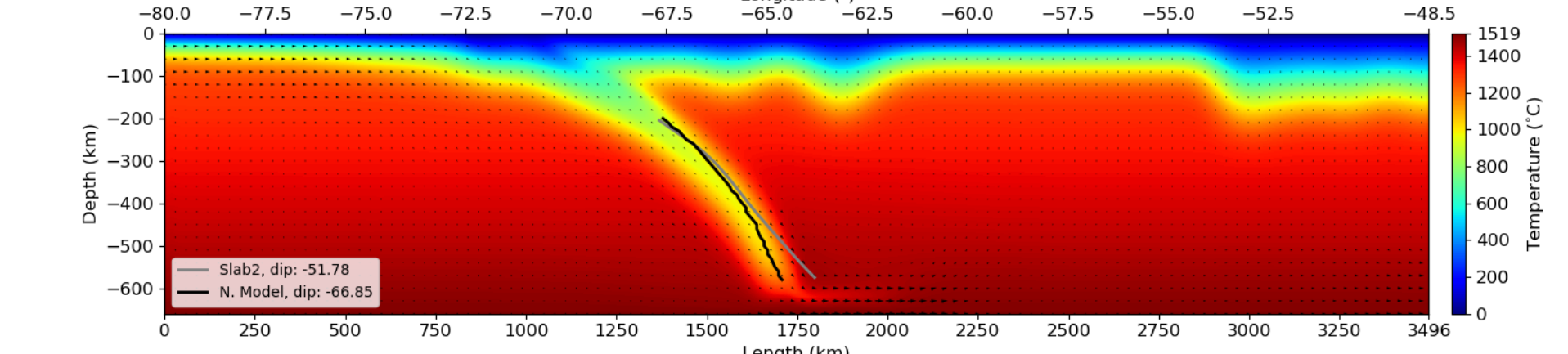
## Results



(a) Thermal structure and velocity field at 0.00 Myr.



(b) Thermal structure and velocity field at 2.50 Myr.



(c) Thermal structure and velocity field at 4.99 Myr.

Figure 4: Temperature and velocity profiles showing the evolution of the dip angle of the subducting slab until 4.99 Myr. The simulation was made using a thicknesses of 85 km for the subducting slab, and 6 km for the oceanic crust. The compositional factors are  $C = 1000$  for the lithosphere,  $C = 1$  for the mantle, and  $C = 0.01$  for the lubricant layer. Densities are  $\rho_m = 3300 \text{ kg/m}^3$  for the mantle,  $\rho_{cc} = 2750 \text{ kg/m}^3$  for the continental crust, and  $\rho_{oc} = 2800 \text{ kg/m}^3$  for the oceanic crust.

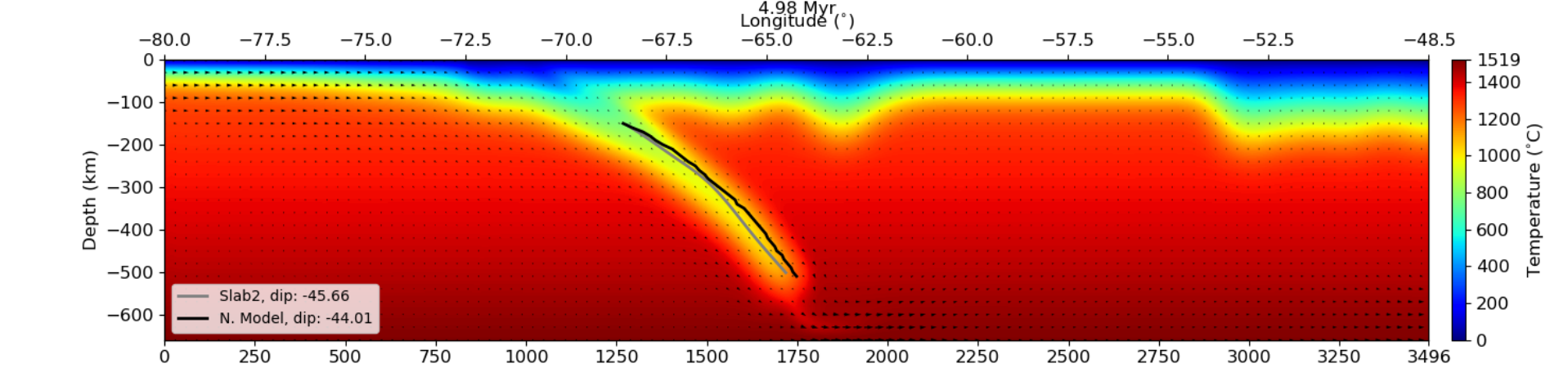


Figure 5: Simulation with the smallest dip angle difference between the Slab2 and the simulation at 4.98 Myr. The thicknesses of the subducting slab and the oceanic crust are 80 and 7 km, respectively. The compositional factors are  $C = 1000$  for the lithosphere,  $C = 1$  for the mantle, and  $C = 0.01$  for the lubricant layer. Densities are  $\rho_m = 3300 \text{ kg/m}^3$  for the mantle,  $\rho_{cc} = 2750 \text{ kg/m}^3$  for the continental crust, and  $\rho_{oc} = 2800 \text{ kg/m}^3$  for the oceanic crust.

## Conclusions

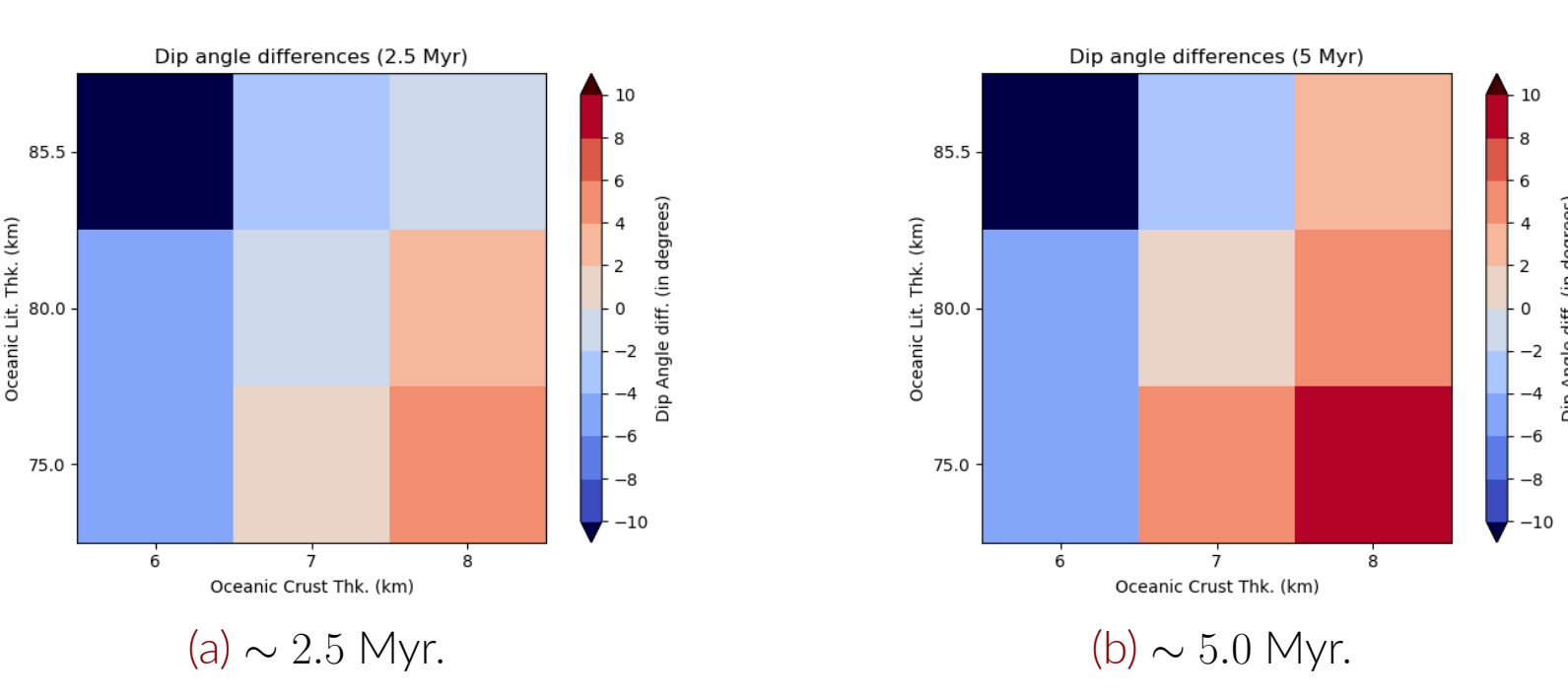


Figure 6: Results for a few combinations of oceanic lithosphere thickness and oceanic crust thickness showing the difference between the dip angles of the simulated subducting slab and the Slab2 model. The difference was calculated at two distinct steps for each simulation.

## References

- [1] Marcelo Assumpção and Gerardo Suárez. Source mechanisms of moderate-size earthquakes and stress orientation in mid-plate South America. *Geophysical Journal International*, 92(2):253–267, 1988.
- [2] Gavin P. Hayes, Ginevra L. Moore, Daniel E. Portner, Mike Hearne, Hanna Flamme, Maria Furtney, and Gregory M. Smoczyk. Slab2, a comprehensive subduction zone geometry model. *Science*, 362(6410):58–61, 2018.
- [3] Brian K. Horton and Peter G. DeCelles. The modern foreland basin system adjacent to the Central Andes. *Geology*, 25(10):895–898, 1997.
- [4] Michael E. Pasyanos, T. Guy Masters, Gabi Laske, and Zhitu Ma. LITHO1.0: An updated crust and lithospheric model of the Earth. *Journal of Geophysical Research: Solid Earth*, 119(3):2153–2173, 2014.
- [5] Victor Sacek. Post-rift influence of small-scale convection on the landscape evolution at divergent continental margins. *Earth and Planetary Science Letters*, 459:48–57, 2017.
- [6] V. S. Solomatov and L. N. Moresi. Scaling of time-dependent stagnant lid convection: Application to small-scale convection on Earth and other terrestrial planets. *Journal of Geophysical Research: Solid Earth*, 105(B9):21795–21817, 2000.
- [7] Naomi Ussami, Shozo Shiraiwa, and José María Landim Dominguez. Basement reactivation in a sub-Andean foreland flexural bulge: The Pantanal wetland. *Tectonics*, 18(1):25–39, 1999.